Investigation of Power Factor Characteristic in Permanent Magnet Motors for In-Wheel Direct Drive Application

Yanlei Yu, *Member*, *IEEE*, Feng Chai, *Member*, *IEEE*, Yulong Pei, Martin Doppelbauer, and Christopher H. T. Lee, *Senior Member, IEEE*

***Abstract*—This paper proposes the intrinsic coefficient of power factor in permanent magnet vernier motors (PMVMs) influenced by slot-pole combinations for in-wheel direct drive application. To start with, the theoretical expression of power factor under typical conditions is derived, and the dominant influencing coefficients are extracted. Secondly, each inductance component is calculated theoretically, eg. air-gap main inductance, slot leakage inductance, etc. Based on previous derivation, the intrinsic coefficient of power factor is extracted, which represents the high-power-factor ability and be utilized in the initial machine design. It is influenced by the armature poles, armature magnetomotive force (MMF) harmonic spectra, winding factor, and air-gap permeance. Moreover, the slot-pole combinations with various high-power-factor ability are illustrated, in which, the ones with coil-pitch of two-slot pitches overwhelm. In order to validate the theoretical analysis, several PMVM model candidates with various slot-pole combinations are selected and simulated by finite-element-analysis (FEA). Finally, the prototype of PMVM with 28p18s and benchmark PMSM with 28p24s were manufactured and tested for experimental validation. Overall, this paper aims to provide a guideline to select the slot-pole combinations with high-power-factor ability, particularly in PMVM, for in-wheel direct drive.**

***Index Terms*——Permanent magnet vernier motor, permanent magnet synchronous motor, power factor, slot-pole combinations, intrinsic coefficient, inductance, in-wheel direct drive.**

I. Introduction

At present, in-wheel drive gains much attention because it can provide distinctive advantages, such as high efficiency, strong vehicle dynamic, and more space within the vehicle by removal of the transmission axis and mechanical components. In-wheel motor unit, as the origin of power, plays an important role. To meet the requirements, in-wheel motors claim to have higher demands of efficiency, torque density, power factor, and wide constant power speed range (CPSR) [1]-[5]. Typically, the power factor will determine the voltage level, volume, and mass of the power supply in electric vehicles (EV), which has a great impact on the vehicle performances, such as the range, charging speed. Thus, the power factor issue in EV can't be ignored.

Recently, permanent magnet vernier motors (PMVM), as one of the flux modulation machines (FMM), are employed as the in-wheel motors due to the inherent higher torque density and simple topology. However, PMVM lose out in terms of power factor compared with PMSM [6]-[10]. In previous researches, low power factor is caused by the high flux modulated armature field and severe flux leakage [11]-[13], so the essential reasons have not revealed, especially the differences of power factor between PMSM and PMVM. From the basic theory, armature reaction reactance is most responsible for the low power factor, which is intrinsically related to the inductances. Generally, for PM machines, *d*-axis inductance can reflect the flux-weakening capability to some extent, while the difference between *d*-axis and *q*-axis inductance can exhibit the value of reluctance torque [14]-[17]. Moreover, the inductances, especially for the *q*-axis inductance, also reflect the ability with high power factor. The larger the inductance is, the lower the high-power-factor ability of the motor is. For PMVM design, the slot-pole combinations will influence the inductance critically. If the potential slot-pole combinations with high-power-factor ability are selected before theoretical calculation and FEA, it helps to promote the design efficiency. Especially for PMVM, the low power factor is the main problem for practical application, so evaluating the power factor is essential when choosing the number of PMs and slots. Hence, the investigation of slot-pole combinations with a high-power-factor ability has significance in practice.

Although the topologies of PMVM and PMSM are in some ways different, but they also have similarities. The inductance features and calculation methods are similar. It is believed that the interior permanent magnet machine (IPM) is superior to obtain the reluctance torque because the difference between L_d and L_q is considerable, whereas El-Refaie has revealed that the surface-mounted permanent magnet machines with fractional-slot concentrated winding (FSCW) can also provide a larger *d*-axis inductance than that with integral-slot distributed winding (ISDW) [19]-[20]. Besides, Juha Pyrhönen et al. has proposed the analytical calculation method of inductance components in tooth-coil PMSM, where the influencing factors of inductance are investigated [21]-[23]. Moreover, it is also noted that the theoretical inductance expression is available when the stator core and rotor core don't get saturated [24]. Up to now, whether the previous studies are suitable to PMVM has not revealed, and the influencing factor of each inductance component in PMVM has not focused on, which should be paid more attention in the future researches.

At present, for in-wheel direct drive, the IPM combined with FSCW has become the common choices for competitive torque and better flux weakening capabilities [25]-[27]. However, the existing researches of *d*-axis inductance between FSCW, ISDW are based on the same PM pole number. If the PM pole number is different, the final results have not revealed yet. Furthermore,

the power factor in PMVM is a key item that depends not only on inductance but also on the other items, eg. current frequency, back-EMF amplitude etc. In addition, the dominant parameters should be targeted for optimization. Thus, exploring the power factor distribution under various slot-pole combinations plays a significant role during the design of PMVM, and the previous papers have not addressed this yet, especially for the practical in-wheel drive applications. D. W. Li et al. have studied the power factor of PMVM and proposed a new modular structure to achieve both high-power-factor and torque capability, where the armature reaction field, especially the flux-modulated ones, dominates the power factor in PMVM [28]-[29]. Nevertheless, the theoretical analysis of high-power-factor ability in PMVM under various gear ratios and slot-pole combinations have not revealed until now. At present, PMSM are still the mainstream products as the in-wheel motors, while PMVM own excellent torque capability and quality but poorer power factor [30]-[31]. Thus, the power factor issue in PMVM is particularly essential.

This paper proposes the intrinsic coefficient of power factor in PMVM with various slot-pole combinations and gear ratios for in-wheel direct drive. In Section II, based on the conditions of in-wheel motors, the expressions of power factor are derived and the influencing factors are summarized. In section III, it is devoted to theoretical calculation of inductance component, and a parameter titled as the "intrinsic coefficient" to represent the high-power-factor ability is proposed and exacted. In Section IV, the models equipped with various slot-pole combinations are established and simulated, where FEA validation for typical ones with high-power factor ability has carried out. In Section V, two prototypes, one PMVM and one PMSM, are tested to verify the correctness of theoretical analysis.

II. Theoretical Derivation of Power Factor

For PM machines, if the reluctance torque can be neglected, I_d=0 control strategy is always applied; if the reluctance torque exists, I_d≠0 control strategy is applied, and the maximum torque per ampere (MTPA) is preferred. For in-wheel motors, it always operates at constant torque or flux-weakening area. The power factor is calculated according to the phasor diagrams in Fig. 1, where θ is the current angle, Ψ is the power angle between phase voltage U and no-load back-EMF E_0, φ is the power factor angle, E_0 is the amplitude of no-load back-EMF, X_d, X_q are the d-axis and q-axis reactance, X_{ad}, X_{aq} are the armature reaction d-axis and q-axis reactance, X_σ is the leakage reactance, I_d, I_q are the d-axis and q-axis current, I_1 is the phase current amplitude, R_a is the phase resistance.

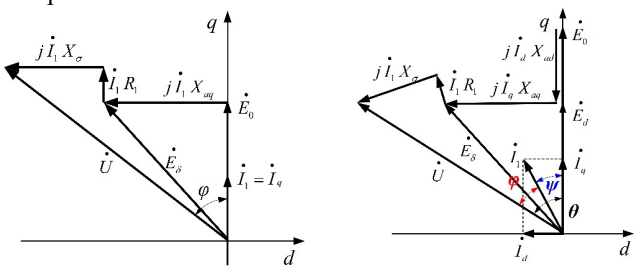

Fig. 1. Phasor diagrams under I_d=0 and I_d<0 control strategies. (a) I_d=0 control strategy. (b) I_d<0 control strategy.

A. Theoretical Expression

In PM machines, the following equations can be obtained.

$$\begin{cases} U\cos\theta = E_0 - I_dX_d + I_qR_a \\ U\sin\theta = I_qX_q + I_dR_a \\ I_q = I_1\cos\psi \\ I_d = I_1\sin\psi \\ \varphi=\theta-\psi \end{cases} \tag{1}$$

Combing equations in (1), if the phase resistance is neglected, the power factor can be written as a function of I_d and I_q, X_d and X_q, E_0, and it can be expressed as

$$\cos\varphi=\cos\left[\operatorname{actan}\left(\frac{I_qX_q}{E_0-I_dX_d}\right)-\arctan\left(\frac{I_d}{I_q}\right)\right] \tag{2}$$

In PMSM, the q-axis reactance and no-load back-EMF can be expressed as follows.

$$X_q = \omega_sL_q \tag{3}$$

$$E_0 = \sqrt{2}\pi f_sN_1\Phi_0k_{w1} \tag{4}$$

where ω_s is the electrical angular speed, L_q is q-axis inductance, f_s is the electrical frequency of current, N_1 is the coil turns of per phase, k_{w1} is the fundamental winding factor, and then Φ_0 is the amplitude of fundamental no-load flux, which can be written as

$$\Phi_0 = B_{av}\tau l_{stk} = \frac{2}{\pi}B_{m1}\tau l_{stk} \tag{5}$$

where B_{av} is the average air-gap magnetic field amplitude, B_{m1} is the fundamental component amplitude of air-gap magnetic field, l_{stk} is the stack length of iron core, τ is the pole pitch. The pole pitch τ and electrical frequency f_s can be written as

$$\tau = \frac{\pi D_{is}}{2N_r} \tag{6}$$

$$f_s = \frac{nN_r}{60} \tag{7}$$

where D_{is} is the inner stator diameter, n is the speed, and N_r is the PM pole pair number. In PMSM, N_r equals to armature pole pair p.

In PMVM, only the open-slot stators are considered and used in the following parts. In terms of [29], the no-load back-EMF can be written as follows.

$$E_0 = \sqrt{2}\pi f_sN_1\Phi_0k_{w-equ}\left(\frac{N_r}{p}\right) = \sqrt{2}\pi f_sN_1\Phi_0k_{w-equ}G_r \tag{8}$$

where $k_{w\text{-}equ}$ is the equivalent winding factor, G_r is the gear ratio (N_r/p). The winding factor $k_{w\text{-}equ}$ can be expressed as

$$k_{w-equ} = k_{w1}\Lambda_1 + \left(\frac{2k_{wv1}}{v_1}\right)\Lambda_0 + \left(\frac{2k_{wv2}}{v_2}\right)\Lambda_1 \tag{9}$$

where v_1, v_2 represent the 1st, 2nd slot harmonic orders, k_{wv1}, k_{wv2} are the winding factors of the 1st, 2nd slot harmonics, which have the same value as the fundamental one, Λ_1, Λ_2 are the 1st, 2nd air-gap relative permeance values. The slot harmonic order can be expressed as

$$v_h = h\left(\frac{Q_s}{p}\right)\pm 1 \tag{10}$$

$$k_{w1} = k_{wv_1} = k_{wv_2} \ldots = k_{wv_h} \tag{11}$$

where k_{wvh} is the winding factor of hth slot harmonic, Q_s is the slot number. Substituting (10) into (9), the equivalent winding factor can be expressed as

$$k_{w-equ}=k_{w1}\left(\Lambda_1+\left(\frac{2}{v_1}\right)\Lambda_0+\left(\frac{1}{v_2}\right)\Lambda_1\right) \tag{12}$$

Then, the equivalent air-gap permeance can be defended as

$$\Lambda_{equ}=\left(\Lambda_1+\left(\frac{2}{v_1}\right)\Lambda_0+\left(\frac{1}{v_2}\right)\Lambda_1\right) \tag{13}$$

If the phase resistance is neglected, by deriving the equations (3)-(7) into (2), the power factor of PMSM can be written as

$$\cos\varphi=\cos\left[\operatorname{actan}\left[\frac{\left(\sqrt{2}pL_q\right)I_q}{\left(D_{is}l_{stk}N_1B_{m1}k_{w1}\right)-\left(\sqrt{2}pL_d\right)I_d}\right]\text{-}\arctan\left(\frac{I_d}{I_q}\right)\right] \tag{14}$$

If the phase resistance is neglected, by deriving the equations (8)-(13) into (2), the power factor of PMVM can be written as

$$\cos\varphi=\cos\left[\operatorname{actan}\left[\frac{\left(\sqrt{2}pL_q\right)I_q}{\left(D_{is}l_{stk}N_1B_{m1}k_{w-equ}\right)-\left(\sqrt{2}pL_d\right)I_d}\right]\text{-}\arctan\left(\frac{I_d}{I_q}\right)\right] \tag{15}$$

If I_d=0 is applied, the power factor can be expressed as

$$\cos\varphi=\frac{1}{\sqrt{1+\left(\frac{I_qX_q}{E_0+I_qR_1}\right)^2}} \tag{16}$$

If the phase resistance is neglected, by deriving the equations (3)-(7) into (16), the power factor of PMSM can be written as

$$\cos\varphi=\frac{1}{\sqrt{1+\left[\frac{\left(\sqrt{2}pL_q\right)I_q}{\left(N_1D_{is}l_{stk}\right)\left(k_{w1}B_{m1}\right)}\right]^2}} \tag{17}$$

If the phase resistance is neglected, by deriving the equations (8)-(13) into (16), the power factor of PMVM can be written as

$$\cos\varphi=\frac{1}{\sqrt{1+\left[\frac{\left(\sqrt{2}pL_q\right)I_q}{\left[\left(N_1D_{is}l_{stk}\right)\left(k_{w-equ}B_{m1}\right)\right]}\right]^2}} \tag{18}$$

In PMVM and PMSM, if the slot-pole combination and basic design dimensions are selected, the inductance can be obtained basically, and then the power factor characteristic is determined generally under the applied control strategy. It indicates that the d-axis and q-axis inductance can affect the power factor a lot in PMVM and PMSM.

B. Influencing Coefficient of Power Factor

From the expressions of power factor, the influencing factors of power factor can be divided into two categories, the design and control parameters, where the stator dimeter D_{is}, axial core length l_{stk}, phase coil turns N_1, d-axis and q-axis inductance L_d, L_q, armature pole pair p, and winding factor $k_{w\text{-}equ}$ belong to the design parameters, and d-axis and q-axis current I_d, I_q belong to the control parameters. Considering the electrical loading, if the design parameters D_{is}, l_{stk}, N_1 are fixed, the air-gap flux density amplitude B_{m1} is also assumed to be same to guarantee the same magnetic loading. Then, the parameters p, L_d, L_q, k_{w1} determine the final power factor, which can be extracted as the influencing coefficient of power factor as follows.

$$\begin{cases} PF_{PMSM}=\dfrac{k_{w1}}{pL_q} \\ PF_{PMVM}=\dfrac{k_{w1}\Lambda_{equ}}{pL_q} \end{cases} \tag{19}$$

It can be extracted that armature pole pair, q-axis inductance, and winding factor are the dominant parameters of power factor, which compose the influencing coefficient of power factor. In the following parts, the determined design parameters of q-axis inductance are further extracted and highlighted.

III. Investigation of Each Inductance Component

Different slot-pole combinations will generate various d-axis and q-axis inductance component, and then produce the d-axis and q-axis armature reaction reactance, which takes the most responsibility for power factor characteristic.

A. Calculation of Inductance Components

In PM machines, the air-gap flux linkage connecting stator and rotor core corresponds to the magnetizing inductance, and leakage flux linkage corresponds to leakage inductance. Thus, the total inductance can be calculated as the sum of magnetizing inductance and leakage inductance. The leakage inductance can be calculated as the sum of air-gap leakage inductance $L_{\delta\sigma}$, slot leakage inductance L_u, tooth tip leakage inductance L_t, and end winding leakage inductance L_e.

For each inductance, the magnetizing inductance and air-gap leakage inductance make up the majority of the total inductance, which indicates that the sum of two components could present the total inductance possibly.

1) Air-Gap Inductance

Air-gap inductance contains the fundamental one of armature reaction inductance and the other harmonic leakage inductances, which can be written as

$$L_{\delta d,\delta q}=L_{md,mq}+L_{\sigma d,\sigma q} \tag{20}$$

where L_{md}, L_{mq} are d-axis and q-axis fundamental inductance, and $L_{\sigma d}$, $L_{\sigma q}$ are d-axis and q-axis harmonic leakage inductance. The harmonic inductance L_{md} and L_{mq} can be written as

$$L_{md,mq}=\left(\frac{m}{\pi}\right)D_{is}l_{stk}\left(\frac{N_1k_{w1}}{p}\right)^2\left(\frac{K_{d,p}}{K_{sd,sp}}\right)\Lambda_{ad,aq} \tag{21}$$

where m is the phase number, $K_{d,\,p}$ is the d-axis and q-axis influencing factor, $K_{sd,\,sq}$ is the d-axis and q-axis saturation factor, $\Lambda_{ad,\,aq}$ is the d-axis and q-axis air-gap permeance.

Similarly, the expression of harmonic leakage inductance is same as the armature reaction inductance, which can be written as follows.

$$L_{\sigma d,\sigma q}=\left(\frac{m}{\pi}\right)D_{is}l_{stk}\left(\frac{N_1k_{wv}}{vp}\right)^2\left(\frac{K_{d,p}}{K_{sd,sp}}\right)\Lambda_{ad,aq} \tag{22}$$

In terms of each inductance component, it can be observed that the MMF harmonic inductance value mainly depends on the selection of the machine design parameters, eg. the phase number, the inner stator diameter, stack length, MMF harmonic

orders, and winding factors. In addition, MMF harmonic orders and winding factors are influenced by the slot-pole combination in PM machines. Hence, the criteria to evaluate the inductance value among various slot-pole combinations can be written as

$$\sum \nu_\sigma = \sum \left(\frac{k_{w\nu}}{\nu} \right)^2 \tag{23}$$

The total harmonic leakage inductance is summed as

$$L_{\delta d,\delta q} = \left(\frac{m}{\pi} \right) D_{is} l_{stk} N_1^2 \left(\sum \nu_\sigma \right) \left(\frac{K_{d,p}}{K_{sd,sp}} \right) \Lambda_{ad,aq} \tag{24}$$

The total harmonic inductance can be expressed as

$$L_{\delta d,\delta q} = C_0 \sum \nu_\sigma \tag{25}$$

where the constant coefficient can be expressed as

$$C_0 = \left(\frac{m}{\pi} \right) D_{is} l_{stk} N_1^2 \left(\frac{K_{d,p}}{K_{sd,sp}} \right) \Lambda_{ad,aq} \tag{26}$$

2) Slot Leakage Inductance

Slot leakage inductance is an inductance created by a real slot leakage flux, which cannot be neglected.

$$L_s = \frac{4m}{Q} \mu_0 l_{stk} \lambda_s N_1^2 \tag{27}$$

The slot permeance factor depends on the geometry of the slot. For the open-slot and semi-closed slot, the slot permeance factor can be written as [21]

$$\lambda_s = k_1 \left(\frac{h_4 - \Delta h}{3b_4} \right) + k_2 \left(\frac{h_3}{b_4} + \frac{h_1}{b_1} + \frac{h_2}{b_4 - b_1} \ln \frac{b_4}{b_1} \right) + \frac{\Delta h}{4b_4} \tag{28}$$

where we can define the parameter as

$$\begin{cases} k_1 = \dfrac{5+3g}{8} \\ k_2 = \dfrac{1+g}{2} \end{cases} \tag{29}$$

3) Tooth Tip Leakage Inductance

The tooth leakage inductance can be expressed as

$$L_t = \frac{4m}{Q_s} \mu_0 l_{stk} \lambda_t N_1^2 \tag{30}$$

where λ_t is the tooth tip leakage specific permeance, which can be written as

$$\lambda_t = k_2 \frac{5\left(\delta / b_1 \right)}{5 + 4\left(\delta / b_1 \right)} \tag{31}$$

where δ is the air-gap length, and b_1 is the slot opening.

4) End Leakage Inductance

End winding leakage flux results in the currents flowing in the end winding [21].

$$L_e = \frac{4m}{Q_s} \mu_0 N^2 q L_{stk} \lambda_e = \frac{2}{p} N^2 \mu_0 l_{stk} \lambda_e \tag{32}$$

where λ_e is the end leakage specific permenace

The end leakage permenaces can be written as [21]

$$\begin{cases} \lambda_e = 0.67 \dfrac{q}{l_{stk}} \left(l_E - 0.64\tau \right) \\ \lambda_e = 0.57 \dfrac{q}{l_{stk}} \left(\dfrac{3\beta\text{-}1}{2} \right) \end{cases} \tag{33}$$

The sum of four inductance components represents the *d*-axis and *q*-axis total inductances. Therefore, the theoretical value of power factor coefficient can be calculated.

B. Intrinsic Coefficient of Power Factor

1) Intrinsic Coefficient Definition

Herein, according to (19), the parameter H is defined as the "intrinsic coefficient" to evaluate the high-power-factor ability.

$$\begin{cases} H_{PMSM} = \dfrac{k_{w1}}{p \sum \nu_\sigma} \\ H_{PMVM} = \dfrac{k_{w1} \Lambda_{equ}}{p \sum \nu_\sigma} \end{cases} \tag{34}$$

where p is the number of PM pole pairs, $\Sigma\nu_\sigma$ is the coefficient of air gap permeance, winding factor, and equivalent coefficient.

2) Intrinsic Coefficient Calculation

For the power factor, $\Sigma\nu_\sigma$ is not the only influencing factor, and the electrical frequency also matters, where it is related to rotor speed and PM pole pair number. Therefore, $p\Sigma\nu_\sigma$ is the determined factor in PM machines, which is true for PMSM and PMVM. If both $\Sigma\nu_\sigma$ and N_r are large in PM machines, its power factor is also not as high as expected. In the following part, the intrinsic coefficients under various slot-pole combinations are calculated to identify the ability to produce high power factor.

The calculation of $\Sigma\nu_\sigma$ is introduced for three-phase windings with a phase belt of 60°, which is shown as follows.

$$\begin{cases} b = \dfrac{Q_s}{\gcd\left(Q_s, 2mp \right)} \\ d = \dfrac{2mp}{\gcd\left(Q_s, 2mp \right)} \end{cases} \tag{35}$$

where gcd (Q_s, m) represents the greatest common divisor of Q_s and $2mp$.

All harmonic orders by armature reaction is written as

$$\nu_s = \begin{cases} \left[\left(6n+1 \right) / d \right] or \left[-\left(6n-1 \right) / d \right], & d \text{ is odd} \\ \left[2\left(3n+1 \right) / d \right] or \left[-2\left(3n-1 \right) / d \right], & d \text{ is even} \end{cases} \tag{36}$$

where n=0, 1 ,2,…

Parameter n_x is the minimum number to make X is an integer, and then the X can be expressed as

$$X = \begin{cases} \left[6b\left(n_x - 1 \right) + 1 \right] / d, & d \text{ is odd} \\ 2\left[3b\left(n_x - 1 \right) + 1 \right] / d, & d \text{ is even} \end{cases} \tag{37}$$

where n_x=0, 1, 2,…. Then, the $\Sigma\nu_\sigma$ can be calculated as

$$\sum \nu_\sigma = \begin{cases} \displaystyle\sum_{n=0,1,2,\ldots}^{\infty} \left[\frac{1}{\nu_s} \sin\left(\nu_s \frac{\pi\beta}{2} \right) \frac{\sin\left(\frac{\pi}{6} \nu_s dH \right)}{b \sin\left(\frac{\pi}{6} \frac{\nu_s dH}{b} \right)} \right], d \text{ is odd} \\ \displaystyle\sum_{n=0,1,2,\ldots}^{\infty} \left[\frac{1}{\nu_s} \sin\left(\nu_s \frac{\pi\beta}{2} \right) \frac{\cos\left(\frac{\pi}{12} \nu_s dH \right)}{b \cos\left(\frac{\pi}{12} \frac{\nu_s dH}{b} \right)} \right], d \text{ is even} \end{cases} \tag{38}$$

The parameter β can be expressed as

$$\beta = \frac{y_1}{mq} \tag{39}$$

TABLE I
THE PARAMETER Σv_σ, H_{PMVM}, H_{PMSM} UNDER DIFFERENT SLOT-POLE COMBINATIONS

Slot Number	Items	Armature pole pair number p							
		2	4	5	7	8	10	11	13
6	$N_r(G_r)$	4 (2)	-	-	-	-	-	-	-
	q	0.5	0.25	0.2	0.143	0.125	0.1	0.091	0.077
	k_{w1}	0.866	0.866	1	-1	-0.866	-0.866	-1	1
	$\sum v_\sigma$	0.273	0.273	1.096	1.096	0.273	0.273	1.096	1.096
	H_{PMSM}	1.587	0.793	-	-	-	-	-	-
	H_{PMVM}	1.272	-	-	-	-	-	-	-
9	$N_r(G_r)$	7 (7/2)	5 (5/4)	-	-	-	-	-	-
	q	0.75	0.375	0.3	0.214	0.188	0.15	0.136	0.115
	k_{w1}	0.945	0.945	0.945	-0.945	-0.945	0.945	0.945	-0.945
	$\sum v_\sigma$	0.283	0.121	0.121	0.283	0.933	0.933	0.283	0.121
	H_{PMSM}	1.669	1.953	1.562	-	-	-	-	-
	H_{PMVM}	1.070	1.410	-	-	-	-	-	-
12	$N_r(G_r)$	10 (5)	8 (2)	7 (7/5)	5 (5/7)	4 (1/2)	2 (1/5)	1 (1/11)	-
	q	1	0.5	0.4	0.289	0.25	0.2	0.182	0.154
	k_{w1}	1	0.866	0.933	0.933	0.866	1	0.933	-0.933
	$\sum v_\sigma$	0.274	0.068	0.068	0.068	0.068	0.205	0.891	0.891
	H_{PMSM}	1.814	3.185	2.746	1.961	-	-	-	-
	H_{PMVM}	1.042	1.946	1.748	-	-	-	-	-
15	$N_r(G_r)$	13 (13/2)	11(11/4)	10 (2)	8 (8/7)	7 (7/8)	5 (1/2)	4 (4/11)	2 (2/13)
	q	1.25	0.625	0.5	0.357	0.313	0.25	0.227	0.192
	k_{w1}	0.951	0.951	0.866	0.951	0.951	0.866	-0.951	-0.951
	$\sum v_\sigma$	0.254	0.078	0.044	0.043	0.043	0.044	0.078	0.254
	H_{PMSM}	1.873	3.049	3.937	3.155	2.762	-	-	-
	H_{PMVM}	1.010	**1.706**	**2.257**	1.919	-	-	-	-
18	$N_r(G_r)$	16 (8)	14 (7/2)	13(13/5)	11(11/7)	10 (5/4)	8 (4/5)	7 (7/11)	5 (5/13)
	q	1.5	0.75	0.6	0.429	0.375	0.3	0.273	0.231
	k_{w1}	0.945	0.945	0.945	0.902	0.945	0.945	0.902	-0.945
	$\sum v_\sigma$	0.233	0.071	0.050	0.03	0.03	0.03	0.03	0.05
	H_{PMSM}	2.028	3.322	3.774	5.000	3.937	3.155	-	-
	H_{PMVM}	1.049	**1.761**	**2.033**	2.793	2.247	-	-	-
21	$N_r(G_r)$	19 (19/2)	17(17/4)	16(16/5)	14 (2)	13(13/8)	11(11/10)	10(10/11)	8(8/13)
	q	1.75	0.875	0.70	0.5	0.438	0.35	0.318	0.269
	k_{w1}	0.953	0.932	0.953	0.866	0.89	0.953	0.953	0.89
	$\sum v_\sigma$	0.239	0.070	0.047	0.022	0.022	0.022	0.022	0.022
	H_{PMSM}	1.992	3.333	4.049	5.618	5.051	4.329	3.937	-
	H_{PMVM}	1.001	**1.704**	**2.092**	2.976	2.710	2.410	-	-
24	$N_r(G_r)$	22 (11)	20 (5)	19(19/5)	17(17/7)	16 (2)	14 (7/5)	13(13/11)	11(11/13)
	q	2	1	0.8	0.571	0.5	0.4	0.364	0.308
	k_{w1}	0.966	1	0.925	0.925	0.866	0.933	0.949	0.949
	$\sum v_\sigma$	0.24	0.068	0.043	0.025	0.017	0.017	0.017	0.017
	H_{PMSM}	2.012	3.676	4.310	7.407	6.369	5.495	5.076	4.202
	H_{PMVM}	0.988	**1.828**	**2.160**	3.774	3.279	2.899	2.717	-

The coefficient of air gap permeance Σv_σ of numerous slot-pole combinations is calculated and listed in Table I. Coil pitch is determined to achieve the largest fundamental winding factor. For combinations with the same SPP values, the coil pitch and fundamental winding factor are omitted because they are same. However, Σv_σ maybe not same due to different pole numbers. Therefore, only q and Σv_σ are presented for the same SPP. The negative k_{dp1} means that magnetic field rotates in the negative direction compared with the positive one. From Table I, several inferences can be drawn as follows.

1) Under the same stator slot number, the coefficients Σv_σ and winding factors of PMSM and PMVM show a cyclical variation. The two adjacent winding factors show alternating positive and negative variations, while the coefficient Σv_σ keeps constant in two periods.

2) Under the same armature pole number, the coefficient Σv_σ of PMVM is larger than that of PMSM, because the armature MMF p_sth harmonic has the largest amplitude and its winding factor is the same as the N_rth harmonic;

3) Under the same slot number, when gear ratio G_r is larger than one, the intrinsic coefficient H_{PMVM} is smaller than H_{PMSM}, which indicates that PMVM have a poor ability to produce high power factor than that of PMSM.

4) Under the same slot number, the larger the gear ratio G_r is, the smaller the H_{PMVM} is, the poorer the ability is to produce a high power factor. This indicates a negative correlation between the gear ratio and the ability to produce high power factor.

5) Under the same armature pole number, FSCW ones have smaller H_{PMVM} and H_{PMSM} than the ISDW and FSDW ones. It shows that the FSCW one owns a lower ability to produce high power factor.

The slot-pole combinations with high power factor in Table I are concluded as follows: 22p/8p15s, 28p/8p18s, 26p/10p18s, 34p/8p21s, 32p/10p21s, 40p/8p24s, 38p/10p24s et. al. The gear

ratios are 2.6, 3.5, 2.6, 4.25, 3.2, 5.0, 3.8 respectively. It shows that the ones with high-power factor seems to have a lower gear ratio, which are generally lower than 5.0. This indicates that the power factor may be competitive with torque capability.

Overall, the intrinsic coefficient is related to the armature pole number, coefficient Σv_σ, and equivalent winding factor in PMVMs. Once the slot-pole combinations are determined, the ability to produce high power factor is also certain. Before the accurate calculation, this method can provide a pre-reference.

IV. FEA Validation

A. Slot-Pole Combination Candidates

In this part, several FEA models with high and low intrinsic coefficients are established to validate the previous theoretical analysis. In Fig. 2, the models MH1~MH8 with high intrinsic coefficients should have high-power-factor ability. Besides, the models ML1~ML4 with low intrinsic coefficients should have low-power-factor ability, as shown in Fig. 3. Furthermore, in order to satisfy the in-wheel direct drive applications, the outer rotor topology with spoke-type PMs is utilized to strengthen the air-gap flux density and torque capability. It is noted that only the models with gear ratio larger than 2.0 are selected here to guarantee the output torque capability. In MH1~MH8, the coil-pitch of two slot-pitches is employed, while the coil-pitch of 4, 5, and 6 is utilized in ML1~ML4. Herein, only the three phase windings are considered under the comparisons.

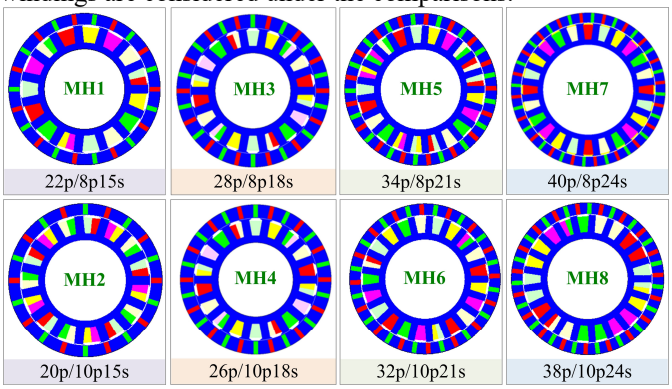

Fig. 2. PMVM model candidates MH1~MH8 with high intrinsic coefficient.

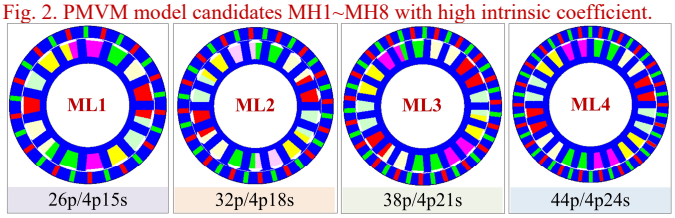

Fig. 3. PMVM model candidates ML1-ML4 with low intrinsic coefficient.

As shown, the design parameters of MH1~MH8, ML1~ML4 are listed in Table II and Table III. It can be observed that the same slot numbers (15, 18, 21, 24) are chosen as the comparison for the ones with high and low intrinsic coefficients. The model with high intrinsic coefficient own low gear ratio and coil-pitch, while the model with low intrinsic coefficient is the opposite.

TABLE II
PARAMETERS OF MH1~MH8 WITH HIGH INTRINSIC COEFFICIENT

Items	MH1	MH2	MH3	MH4	MH5	MH6	MH7	MH8
Q_s	15	15	18	18	21	21	24	24
N_s	15	15	18	18	21	21	24	24
p	8	10	8	10	8	10	8	10
N_r	22	20	28	26	34	32	40	38
y_1	2	2	2	2	2	2	2	2
G_r	2.6	2.0	3.5	2.6	4.25	3.2	5.0	3.8
H	1.71	2.26	1.76	2.03	1.70	2.09	1.83	2.16

TABLE III
PARAMETERS OF MH1~MH8 WITH HIGH INTRINSIC COEFFICIENT

Items	ML1	ML2	ML3	ML4
Q_s	15	18	21	24
N_s	15	18	21	24
p	2	2	2	2
N_r	13	16	19	22
y_1	4	4	5	6
G_r	6.5	8.0	9.5	11.0
H	1.01	1.05	1.00	0.99

B. Calculation of d-axis and q-axis Inductances

The d-axis and q-axis inductances of MH1~MH8 calculated by theoretical method and FEA are compared and shown in Table IV. It can be seen that the d-axis inductance is similar as q-axis inductance in MH1~MH8, which indicate that in PMVM the reluctance torque can be neglected. Besides, MH5, MH7 have a relatively higher inductance among all models.

In the models of ML1~ML4, the d-axis and q-axis inductance are generally larger than these in MH1~MH8. From the power factor expression, the larger the q-axis inductance is, the lower the power factor will be. It can support our previous analysis.

TABLE IV
INDUCTANCE PARAMETERS OF MH1~MH8, ML1~ML4.

Items	Methods	MH1	MH2	MH3	MH4
L_d(mH)	2D FEA	0.72	0.68	0.89	0.76
	Cal.	0.74	0.66	0.84	0.72
L_q(mH)	2D FEA	0.72	0.67	0.76	0.75
	Cal.	0.70	0.63	0.71	0.73
Items	Methods	MH5	MH6	MH7	MH8
L_d(mH)	2D FEA	1.23	0.73	1.34	0.89
	Cal.	1.21	0.70	1.32	0.88
L_q(mH)	2D FEA	0.71	1.31	0.87	0.71
	Cal.	0.67	1.23	0.85	0.69
Items	Methods	ML1	ML2	ML3	ML4
L_d(mH)	2D FEA	1.98	2.24	2.78	2.95
	Cal.	2.02	2.31	2.82	3.04
L_q(mH)	2D FEA	1.97	2.22	2.79	2.94
	Cal.	1.95	2.27	2.74	3.14

C. Power Factor and Torque

1) The Models with High Intrinsic Coefficient

The power factor and torque curves versus with phase current in each model is listed and compared are shown in Fig. 4. It can be seen that the power factors of MH1~MH8 are generally high when the phase current is below the rated current. When the motors operate at over-load condition, the power factor of all models is higher than 0.60. However, the torque capability in M2 is lower than the other ones.

Besides, under the same slot number, the more the armature pole is, the higher the power factor is. Nevertheless, for torque capability, under the same stator slot number, the more PM pole pair is and the larger the gear ratio is, the larger output torque is. This indicates that the power factor and torque in PMVMs are mutually constrained, even though all models have a higher power factor than the other slot-pole combinations. Moreover, the power factor range of M1~M8 keeps at an acceptable value, from 0.60~0.95, which can demonstrate the theoretical analysis of intrinsic coefficient of power factor.

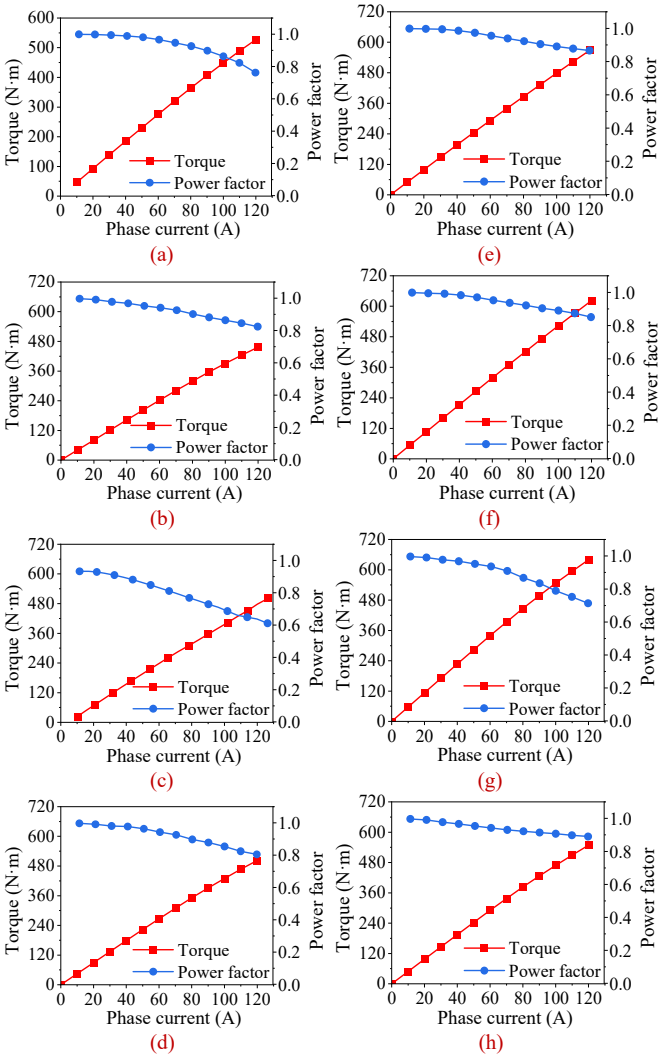

Fig. 4. Power factor versus with phase current under I_d=0 control. (a) MH1. (b) MH2. (c) MH3. (d) MH4. (e) MH5. (f) MH6. (g) MH7. (h) MH8.

2) The Models with Low Intrinsic Coefficient

In Fig. 5, the power factor and torque variation of ML1~ML4 versus with phase current are plotted and compared. It can be seen that the power factors are obviously smaller in ML1~ML4 compared with MH1~MH8. For example, under the same phase current I_{rms}=80A, the power factors of ML1~ML4 are 0.82, 0.84, 0.72, and 0.66, respectively. It can be obviously seen that the power factors are lower than these in MH1~MH8.

From the analysis above, it is obvious that the models with low intrinsic coefficients, i.e., ML1~ML4, indeed have a lower power factor than the models with high intrinsic coefficients, i.e., MH1~MH8, under the same phase current. This means that the higher the intrinsic coefficient is, the higher the power factor is in these models, which can also prove our theoretical analysis before. Therefore, when we select the slot-pole combinations of PMVM, this criterion of high-power-factor ability determined by intrinsic coefficient can be regarded as one of the most useful design guidelines during the motor design, which can make sure that the power factor can be acceptable for in-wheel direct drive. Furthermore, the torque and power factor in these models are always negative correlated. Although ML1~ML4 have lower power factor, the torque capability is superior with larger gear ratio and end length. However, for in-wheel drive, power factor or torque are not the only considerations, some other items, e.g., end length, efficiency, flux weakening capability, should also be carefully considered.

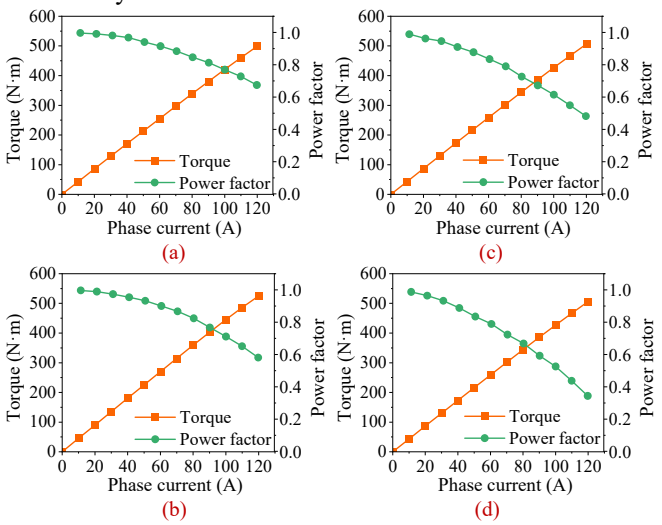

Fig. 5. Power factor versus with phase current under I_d=0 control. (a) ML1. (b) ML2. (c) ML3. (d) ML4.

V. Experimental Validation

A. Prototypes and Experimental Rig

In Fig. 6, the mechanical parts of MH3 and assembly with 16-inch tire are exhibited. It adopts 18 slots with semi-open slot topology for a better overall performance, and 8 armature pole is utilized to compose an 8p18s stator winding. The spoke-type rotor topology is adopted here with 28 magnet poles. The prototype is connected to a 16-inch tire by a hub bearing.

Fig. 6. Mechanical parts prototype MH3 and assembly with 16-inch tire.

TABLE V
THE DESCRIPTIONS OF EXPERIMENTAL EQUIPMENT.

Items	Descriptions
Controller	KEB F5
Torque sensor	JN33-2000
Temperature recorder	YOKOGAWA
Power analyzer	YOKOGAWA WT 5000
Current/Voltage sensors	YOKOGAWA, 200A
PC (Upper computer)	Lenovo, 16G, intel i5

Based on the theoretical and FEA analysis, a prototype with high power factor MH3 was manufactured. The experimental rig is shown in Fig. 7. A conventional PMSM is utilized here as the load motor. Moreover, it also works as a reference of MH3, which can verify the power factor and torque performance. The

YOKOGAWA Analyzer is employed for acquisition of phase current and phase voltage waveforms. The specific experiment testbed is shown in Table V.

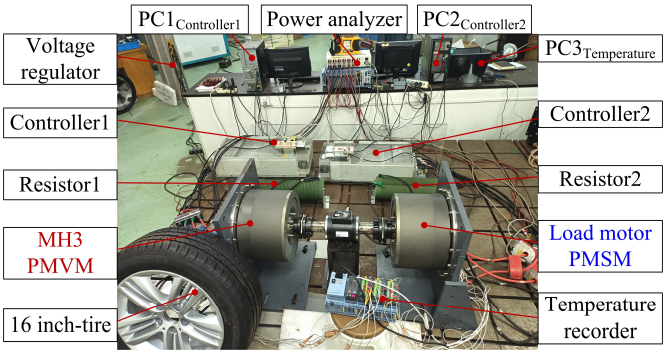

Fig. 7. Experimental rig of PMVM and benchmark PMSM prototypes.

B. Inductance Measurement

The phase resistance R_a, d-axis and q-axis inductance L_d, L_q are measured and shown in Table VI. The inductance of PMVM is larger than that of PMSM, which indicates that the reactance is also larger and the power factor is lower.

TABLE VI
PHASE RESISTANCE AND INDUCTANCE COMPARISON BETWEEN CALCULATED AND EXPERIMENTAL RESULTS

Motor type	Method	L_d (mH)	L_q (mH)	R_1 (mΩ) (T_1=20°C)	R_1 (mΩ) (T_2=150°C)
Conventional PMSM	FEA	0.331	0.448	-	-
	Exp.	0.369	0.506	27.71	36.27
	Error	9.1%	11.5%	-	-
MH3 PMVM	FEA	0.892	0.764	-	-
	Exp.	0.829	0.812	34.44	45.08
	Error	-6.4%	6.0%	-	-

C. Power Factor and Torque Measurement

1) Power Factor

The power factor of PMVM versus with d-axis and q-axis current are shown in Fig. 8. It can be seen that the power factor increases firstly and then decreases with the d-axis and q-axis current. With the increase of d-axis current, the q-axis current at the peak power factor point moves higher. For the condition I_d=0 control, it exhibits that the experimental results match well with the theoretical one, and the error is 8.7% when I_{rms} is 80A.

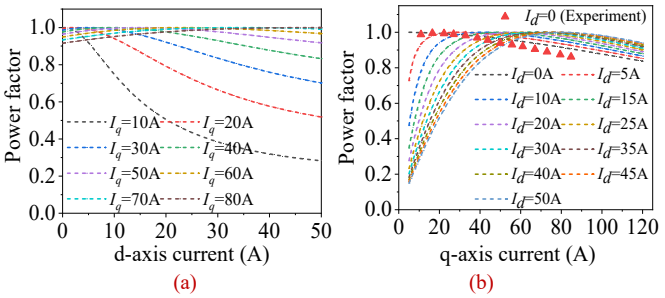

Fig. 8. Power factor versus d-axis and q-axis curves. (a) Power factor vs. d-axis current. (b) Power factor vs. q-axis current.

In order to further compare the power factor of PMVM and conventional PMSM, the power factor curves versus with phase current under I_d=0 control by FEA and experiments are shown in Fig. 9. It can be seen that the experimental results have a good agreement with FEA. Besides, the power factor of PMSM under the same phase current is obviously higher than that of PMVM. When the phase current is 80A, the power factors of PMSM and PMVM are 0.94 and 0.78, respectively.

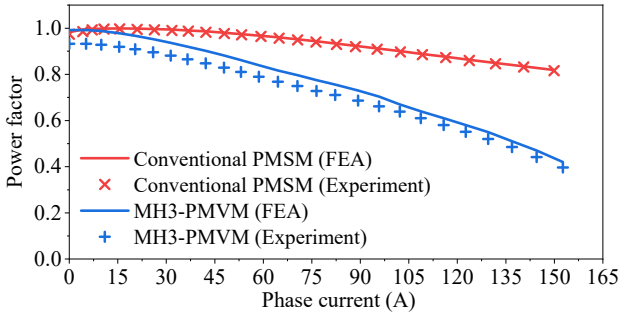

Fig. 9. Power factor versus with phase current curves. (n=550r/min)

The power factor maps of PMVM and PMSM are shown in Fig. 10. It shows that the high-power factor area in the proposed PMVM is considerable compared with that in PMSM, but the high-power-factor area in PMVM under the high speed (350~1200r/min) and high torque (250~650N·m) is still smaller than that in PMSM. Nevertheless, the power factor under the low-speed (0~350r/min) and high-torque (250~650N·m) is higher compared with PMSM surprisingly.

In the area of 800~1200r/min and 300~400Nm, the power factor of PMVM is a bit lower than that of conventional PMSM. We assume that all controllers have the same specifications for a fair comparison. The phase voltage of PMVM is higher under the same speed and torque due to the lower power factor, so the maximum speed and output torque of PMVM are lower than these of conventional PMSM. Then, for in-wheel direct drive, the speed range and vehicle dynamics for climbing will be challenged. In addition, previous references claims that PMVM has a larger torque capability. It means that PMVM can produce a larger torque than PMSM under the same phase current, so PMVM needs a smaller phase current under the same output torque. In fact, due to the low power factor, the phase current of PMVM can be larger than that of PMSM under the same output active power. So, the high torque advantage of PMVM can be weakened by the low power factor.

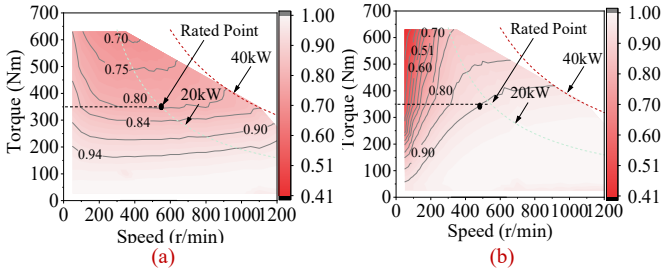

Fig. 10. Power factor maps. (a) MH3-PMVM. (b) Conventional PMSM.

2) Torque Performance

In Fig. 9, the output torque curves of prototype PMVM and PMSM are measured, where the FEA results match well with the experiments. It indicates that the theoretical analysis, FEA, and experiment can be trusted. Besides, the torque capability of PMVM is a little bit larger than that of PMSM, which can also validate that the torque capability is superior compared with PMSM although the power factor of PMVM is much poorer.

Besides, taking account of all analysis above, considering the torque capability, high-power-factor ability, end length, as well as the other performances, it can be concluded that PMVM with high intrinsic coefficient and two-slot pitches is the competitive

candidate for in-wheel drive, which can provide an alternative instead of conventional PMSM during the design.

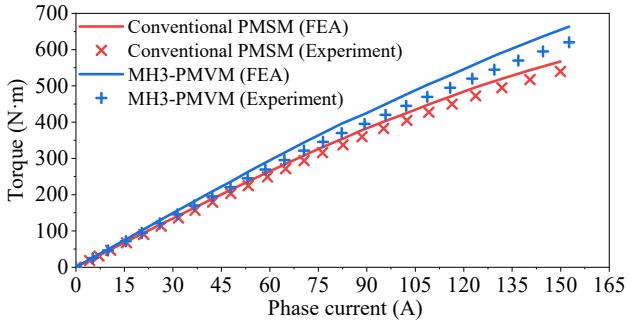

Fig. 11. Torque curve comparison versus with phase current between MH3 and conventional PMSM (n=550r/min).

VI. Conclusion

In this paper, the power factor in PMVMs influenced by slot-pole combinations has revealed. Then, the intrinsic coefficient is extracted to evaluate the high-power-factor ability in PMVM. Then, the conclusions can be summarized as follows.

1) The sum of magnetizing and leakage inductances was defined as the air-gap inductance and extracted as an iteration of variable part Σv_σ and constant part C_0, so that the ability to generate high-power-factor of PMVM under various slot-pole combinations can be quantified.

2) With the definition and calculation of intrinsic coefficient, for PMVM with open-slot stator, the larger the armature pole is, the greater the ability to produce high power factor. Moreover, the output torque has conflict with the power factor ability.

3) The typical slot-pole combinations of PMVM with high power factor are summarized, which contains but not only the following ones: 22p/8p15s, 28p/8p18s, 26p/10p18s, 34p/8p21s, 32p/10p21s, 40p/8p24s, 38p/10p24s et. al. The gear ratio ranges from 2~5, and the end length is relatively short and suitable for in-wheel direct drive application.

4) For power factor, PMVM with high-power-factor ability overwhelm in the area of low-speed and high-torque compared with the conventional PMSM, while it loses out in the area of high-speed and high-torque area.

5) The inherent low power factor of PMVM can be explained from the distribution of proposed intrinsic coefficient. The slot-pole combinations with high power factor ability in PMVM can be determined by the intrinsic coefficient. Besides, the slot-pole combinations of PMVM with coil-pitch of two slot pitches have competitive power factor and torque, which are promising for in-wheel direct drive application.

References

[1] S. U. Chung, S. H. Moon, D. J. Kim, and J. M. Kim, "Development of a 20-Pole-24-Slot SPMSM With Consequent Pole Rotor for In-Wheel Direct Drive," *IEEE Trans. Ind. Electron,* vol. 63, pp. 302-309, Jan 2016.

[2] A.EL-Refaie,"Fractional-slot concentrated-windin synchronous permanent magnet machines: Opportunities and challenges," *IEEE Trans. Ind. Electron*., vol. 57, no. 1, pp. 107-121, Jan. 2010.

[3] P. X. Liang, F. Chai, Y. L. Pei, and L. Chen, " Analytical Model of a Spoke-Type Permanent Magnet Synchronous In-Wheel Motor With Trapezoid Magnet Accounting for Tooth Saturation," *IEEE Trans. Ind. Electron*., vol. 70, no. 7, pp. 7141-7152, Aug. 2019.

[4] J. Cros and P. Viarouge, "Synthesis of high performance PM motors with concentrated windings," *IEEE Trans. Ener. Convers*., vol. 17, no. 2, pp. 248-253, Jun. 2002.

[5] S. Cai, J. L. Kirtley Jr., and C. H. T. Lee, "Critical review of direct-drive electrical machine systems for electric and hybrid electric vehicles," *IEEE Trans. Ener. Convers*., vol. 37, no. 4, pp. 2657-2668, Dec 2022.

[6] J. Zhu, Y. Zuo, H. Chen, J. Chen, and C. H. T. Lee, "Deep-investigated analytical modeling of a surface permanent magnet vernier motor," *IEEE Trans. Ind. Electron.*, vol. 69, no. 12, pp. 12236-12347, Dec 2022.

[7] A. T., T. A. Lipo, "Generic Torque-Maximizing Design Methodology of Surface Permanent-Magnet Vernier Machine," *IEEE Trans. Ind. Appl.*, vol. 36, no. 6, pp. 1539-1546, 2000.

[8] C. H. Lee, "Vernier motor and its design," *IEEE Trans. Pow. Appl, Sys*, vol. PAS-82, no. 66, pp. 343–349, 1963.

[9] Y. Liu, H. Y. Li, Z. Q. Zhu, "A High-Power Factor Vernier Machine with Coil Pitch of Two Slot Pitches". *IEEE Trans. Magn.*, vol.54, no. 11, pp. 778-785, May 2018.

[10] D. W. Li, T. J. Zou, R. H. Qu, D. Jiang, "Analysis of Fractional-Slot Concentrated Winding PM Vernier Machines with Regular Open-Slot Stators", *IEEE Trans. Ind. Appl.*, vol. 54, no. 2, pp. 1320-1330, Mar. 2018.

[11] D. Y. Wu, Z. X. Xiang, and X. Y. Zhu. "Optimization Design of Power Factor for an In-Wheel Vernier PM Machine From the Perspective of Air-Gap Harmonic Modulation," *IEEE Trans. Ind. Electron*., vol. 68, no. 10, pp. 9265-9275, 2022.

[12] L. Xu, W. J. Wu, and W. X. Zhao, "Airgap Magnetic Field Harmonic Synergetic Optimization Approach for Power Factor Improvement of PM Vernier Machines," *IEEE Trans. Ind. Electron*., vol. 69, no. 12, pp. 9265-9275, 2022.

[13] K. K. Du, L. Xu, W. X. Zhao, G. H. Liu, "Analysis and Design of a Fault-Tolerant Permanent Magnet Vernier Machine with Improved Power Factor," *IEEE Trans. Ind. Electron*., vol. 69, no. 5, pp. 4353-4363, 2022.

[14] R. G. Ni, G. L. Wang, X. G. Gui, and D. G. Xu, "Investigation of d- and q-Axis Inductances Influenced by Slot-Pole Combinations Based on Axial Flux Permanent-Magnet Machines," *IEEE Trans. Ind. Elecron*., vol. 61, no. 9, pp. 4539-4551, Sep. 2014.

[15] K. Lee, H. Lee, J. Lee, and W. Kim, "Analysis of Motor Performance According to the Inductance Design of IPMSM," *IEEE Trans. Magn*., vol. 51, no. 3, pp. 1-5, Mar. 2015.

[16] Seun Guy Min, B. Sarlioglu, "Analysis and Comparative Study of Flux Weakening Capability in Fractional-Slot Concentrated Windings," *IEEE Trans. Ener. Convers*., vol. 33, no. 3, pp. 1025-1035, Sep. 2018.

[17] B. Nanda, P. Kumar, "Qualitative and Quantitative Analysis of Different Inductance Measurement Techniques for IPM Synchronous Machines," *IEEE Trans. Ener. Convers*, vol. 36, no. 4, pp. 3305-3316, Dec. 2021.

[18] A.El-Refaie, Z. Q Zhu, T. Jahns, and D. Howe, "Winding inductances of fractional slot surface-mounted permanent magnet brushless machines," *in Conf. Rec. IEEE IAS Annu. Meet*., pp. 1-8, 2008.

[19] A. M. El-Refaie and T. M. Jahns, "Optimal flux weakening in surface PM machines using fractional-slot concentrated windings," *IEEE Trans. Ind. Appl.*, vol. 41, no. 3, pp. 790-800, May/Jun. 2005.

[20] A. M. El-Refaie and T. Jahns, "Scalability of surface PM machines with concentrated windings designed to achieve wide speed ranges of constant power operation,"*IEEE Trans. Energy Convers*.,vol. 21, no. 2, pp. 362-369, Jun. 2006.

[21] J. Pyrhönen, T. Jokinen, and V. Hrabovcová, *Design of Rotating Electrical Machines*. Hoboken, NJ, USA: Wiley, 2008.

[22] P. Ponomarev, P. Lindh, and J. Pyrhönen, "Effect of slot-and-pole combination on the leakage inductance and the performance of tooth-coil permanent-magnet synchronous machines," *IEEE Trans. Ind. Electron*., vol. 60, no. 10, pp. 4310-4317, Oct. 2013.

[23] J. Pyrhönen, V. Ruuskanen, J. Nerg, J. Puranen, H. Jussila, "Permanent-magnet length effects in ac machines," *IEEE Trans. Magn*., vol. 46, no. 10, pp. 3783-3789, Oct. 2010.

[24] B. Stumberger, G. Stumberger, D. Dolinar, A. Hamler, and M. Trlep, "Evaluation of saturation and cross-magnetization effects in interior permanent-magnet synchronous motor," *IEEE Trans. Ind. Appl*., vol. 39, no. 5, pp. 1264-1271, 2005.

[25] A. Tessarolo, M. Mezzarobba, R. Menis, "Modeling, Analysis, and Testing of a Novel Spoke-Type Interior Permanent Magnet Motor With Improved Flux Weakening Capability," *IEEE Trans. Magn*., vol. 51, no. 4, pp. 1-5, Apr. 2015.

[26] D. Y. Wu, Z. X. Xiang, X. Y. Zhu, "Optimization Design of Power Factor for an In-Wheel Vernier PM Machine From the Perspective of Air-Gap Harmonic Modulation," *IEEE Trans. Ind. Electron*., vol. 68, no. 10, pp. 9265-9276, 2021.

[27] Y. Tang, F. Chai, and L. Chen, "Investigation of Open-Circuit Fault-

Tolerant Strategy in a Modular Permanent Magnet Synchronous In-Wheel Motor Based on Electromagnetic-Thermal Analysis," *IEEE Trans. Transp. Electrific*., vol.70, no. 7, pp. 7141-7152, Aug. 2022.
[28] Y. Zhao, D. W. Li, X. Ren, R. H. Qu, "Investigation of Permanent Magnet Vernier Machines From Armature Field Perspective," *IEEE Trans. Ind. Appl*., vol. 10, no. 3, pp. 2934-2945, Feb. 2021.
[29] Y. Zhao, D. W. Li, X. Ren, T. J. Zou, and R. H. Qu, "Design Trade-off Between Torque Density and Power Factor in Surface-Mounted PM Vernier Machines Through Closed-Form Per-Unit Equations," *IEEE Trans. Ind. Electron*. DOI: 10.1109/TIA.2023.3245586, 2022.
[30] Y. L. Yu, F. Chai, Y. L. Pei, M. Doppelbauer, "Performance Comparison Between Permanent Magnet Synchronous Motor and Vernier for In-wheel Direct Drive", *IEEE Trans. Ind. Electron.*, vol. 70, no. 8, pp. 7761-7772, Aug. 2023.
[31] J. Herman, J. Bojkovski, R. Fišer, and K. Drobnič, "An Improved Design of Synthetic Loading Method for a Rapid In-Wheel Motor Characterization in Different Operating Points," *IEEE Trans. Transp. Electrific*., vol. 7, no. 4, pp. 2562-2575, Jun. 2021.

Yanlei Yu received the B.E. degree in automation from Chongqing University, Chongqing, China, in 2016, and the Ph.D. degree in electrical engineering from Harbin Institute of Technology, Harbin, China, in 2022, respectively.
From 2020 to 2021, he worked for the Sino-Germany Research Project for one-year joint Ph.D. study at the Institute of Electrical Engineering, Karlsruhe Institute of Technology, Karlsruhe, Germany. He is a Research Fellow with the School of Electrical and Electronic Engineering, Nanyang Technological University, Singapore. His research interests mainly include the design of high-torque and high-power density permanent magnet machines and drives, novel electrical machine design, multi-physics analysis of permanent magnet machines, especially for the electric propulsion systems.

Feng Chai (M'13) received the B.E. degree from Xi'an Jiaotong University, Xi'an, China, in 1994, and the M.E. and Ph.D. degrees from Harbin Institute of Technology, Harbin, China, in 1998 and 2003, respectively, all in electrical engineering.
She is currently a Professor of Electrical Engineering with Harbin Institute of Technology. Her research interests include electromagnetic field computation, particularly in relation to permanent-magnet machines.

Yulong Pei received the B.E. degree, M.E. degree, and Ph.D. degree all in electrical engineering from Harbin Institute of Technology, Harbin, China, in 2002, 2004, and 2009, respectively.
He is currently an Associate Professor of Electrical Engineering with Harbin Institute of Technology. His research interests include the electromagnetic design of electrical machines, particularly on permanent-magnet machines.

Martin Doppelbauer was born in Germany in 1965. He received the Dipl.-Ing. and Dr.-Ing. degrees in electrical engineering from Technical University of Dortmund, Dortmund, Germany, in 1990 and 1995, respectively. From 1995 to 2010, he was with the Danfoss Bauer, Esslingen, Germany and with SEW Eurodrive, Bruchsal, Germany, in the field of industrial electric motor development.
His research interest includes the electrical drive train of vehicles with a particular focus on electric machines with high power density. Prof. Doppelbauer is also active in the field of standardization and is currently the Chairman of the Technical Committee 2 (Rotating Machinery) of the International Electrotechnical Commission in Geneva. He holds the chair of hybrid and electric vehicles with the Karlsruhe Institute of Technology (KIT), in 2011.

Christopher H. T. Lee (M'12-SM'18) received his B.Eng. (First Class Honors) degree, and Ph.D. degree both in electrical engineering from Department of Electrical and Electronic Engineering, The University of Hong Kong, Hong Kong.
He currently serves as an Assistant Professor at Nanyang Technological University, Singapore and Honorary Assistant Professor at The University of Hong Kong, Hong Kong. He was a Postdoctoral Fellow and then a Visiting Assistant Professor at Massachusetts Institute of Technology, United States. He is an Associate Editor for IEEE Transactions on Industrial Electronics, IEEE Transactions on Energy Conversion, IEEE Access, and IET Renewable Power Generation. He is a Chartered Engineer in Hong Kong. His research interests include Electric Machines and Drives, Renewable Energies, and Electromechanical Propulsion Technologies. In these areas, he has published 1 book, 3 books chapters, and over 160 referred papers.
Dr. Lee has received many awards, including JSPS Fellowship, MDPI Energies Young Investigator Award, NRF Fellowship, Nanyang Assistant Professorship, Li Ka Shing Prize (the best Ph.D. thesis prize) and Croucher Foundation Fellowship.